Journal of Structural Geology, Vol. 13, No. 4, pp. 471 to 483, 1991
Printed in Great Britain

0191-8141/91 $03.00+0.00
© 1991 Pergamon Press plc

Boundary migration and kinking in sheared naphthalene

P. R. BLUMENFELD and C. J. L. WILSON

Department of Geology, University of Melbourne, Parkville, Victoria 3052, Australia

(*Received* 2 *January* 1990; *accepted in revised form* 22 *August* 1990)

Abstract—Deformation of melt-grown anisotropic crystal aggregates of naphthalene with strong [*b*] axis crystallographic preferred orientations produces two distinct microstructural features. The crystals, grown in thin sections, have been constrained to deform in simple shear at $T > 0.9\ T_m$ with the [*b*] axis oblique to the shear direction. In the shortening field the microstructure evolves through crystal kinking with migration of the kink band boundaries. In the stretching field, migration of boundaries induces the development of brittle–ductile shear bands. Kinking and grain boundary migration complement the dominant [*b*] intracrystalline slip in order to accommodate the imposed simple shear at the crystal scale and are similar to the accommodation processes involved in a polycrystal when grain boundary sliding is inactive.

INTRODUCTION

PLASTIC deformation of polycrystalline aggregates is often influenced by compatibility problems between the deformation of the different crystals calling for accommodation processes. Accommodation processes are: (i) sliding along non-coherent boundaries producing spinning and translation of adjacent crystals; (ii) migration of grain boundaries; and (iii) kinking of the crystals.

Understanding these accommodation processes has a very practical impact as they can have significant effects on the development of lattice fabrics. The Taylor–Bishop–Hill model (Lister *et al.* 1978) is based on free lattice spinning of the crystals in a homogeneously deforming polycrystal and does not require any accommodation process. In real polycrystalline aggregates, it is generally considered that grain boundary sliding com plements lattice spinning and intracrystalline slip (Poirier 1985). Gapais & Cobbold (1987) favour kinking in a purely kinematic model of rotation recrystallization, whereas Jessell (1986) favours grain boundary migration in a dynamic model of migration recrystallization. Each of these models can account for the common crystallographic fabric patterns observed in natural materials.

The aim of this paper is to illustrate the processes that accommodate deformation in an anisotropic grain aggregate where grain boundary sliding is impeded. We use the technique of synkinematic microscopy of naphthalene constrained to deform in simple shear (Means 1989). We emphasize the important role of kinking and grain boundary migration, occurring in differently oriented polycrystals, for the same *P*,*T* conditions.

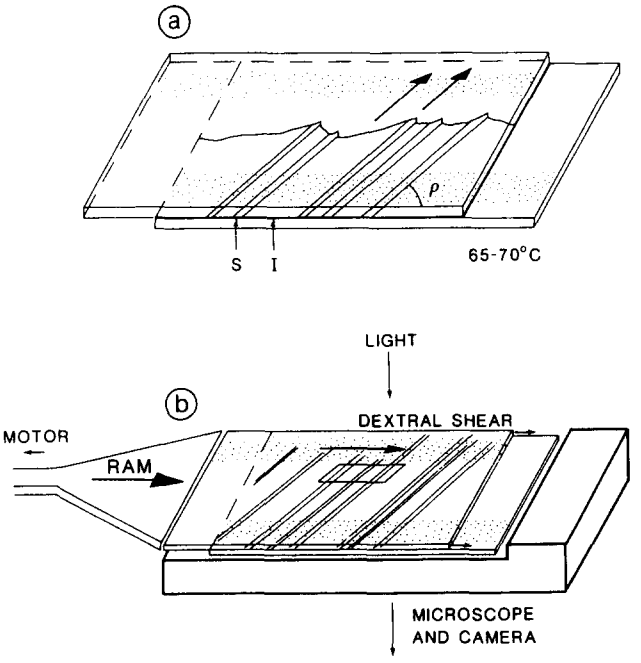

Fig. 1. Experimental techniques. (a) Skeletal growth from a quenched melt of a thin naphthalene sheet between the two window glasses. Note the alternating narrow skeletal (*S*) and interskeletal (*I*) crystals growing along a common direction parallel to the grain boundaries. The angle (ρ) is the initial orientation of intergrowth with respect to shear direction. (b) Deformation stage used in the experiments. Dotted bands represent the frosted areas of the upper and lower glasses and the distance between these is 4 mm. The small rectangle area is an example of the region from where data were recorded during a deformation.

EXPERIMENTAL PROCEDURE

Experimental apparatus

The transmitted light plane deformation apparatus (Fig. 1b) used in this investigation was designed by Urai (1987) and mounted on a Zeiss invertoscope. We used melt-grown samples of 99% pure naphthalene in the simple shear configuration described by Jessell (1986) or Means (1989). Experiments were undertaken in the temperature range 40–80°C (>0.9 m, Table 1). Average shear strain rates were $3 \times 10^{-4}\ s^{-1}$ and the development of the microstructure was followed by time-lapse 16 and 35 mm photography.

Table 1. Summary of chemical and mechanical properties of naphthalene from (1) Wyckoff (1971), (2) Sundararajan (1936), (3) Robinson & Scott (1967), (4) Matvienko *et al.* (1979), (5) Robinson & Scott (1970), (6) Williams & Thomas (1967)

Composition	$C_{10}H_8$: two fused benzene rings, first member of a series of condensed aromatic compounds Anthracene $C_{14}H_{10}$, three fused benzene rings		
Melting and boiling point	80.28°C 217.9°C at 1 atm		
Crystal symmetry and unit cell parameters	monoclinic $a_0 = 8.235$ Å $b_0 = 6.003$ Å $c_0 = 8.658$ Å	$\beta = 122°55'$	(1)
Crystal habit	thin tabular plates parallel to (001) perfect cleavage = {001}		
Optics	$\alpha = 1.52\ \beta = 1.72\ \gamma = 1.94$ for $\lambda = 0.54\ \mu$m (green) 2V = 97° (Biaxial negative) very high birefringence = $\gamma - \alpha = 0.42$ and 0.15 in (001) orientation of the indicatrix: β parallel to [b] $\alpha \wedge [a] = +23°$		(2)
Slip systems		Resolved shear stress (g mm^{-2}) at 27°C:	
basal	(001) [010]	6–13—depending on impurity content (3)	
basal	(001) ⟨110⟩	6–strongly increased by impurities at $T < T_{room}$	(3)
non-basal	(100) [001]	≥80 (4)—560 in anthracene (5)	
non-basal	(100) [010]	predicted (6)—≥259 in anthracene (5)	
non-basal	(010) [001]	predicted (6)—≥184 in anthracene (5)	
non-basal	(010) [100]	predicted (6)—490 in anthracene (5)	
non-basal	{111} ⟨1$\bar{2}$1⟩	observed (4)	

Starting material and crystallography

Naphthalene is an aromatic hydrocarbon with two fused benzene rings (Table 1) that crystallizes below 80°C as monoclinic crystals (Wyckoff 1971) with perfect basal cleavage. The samples for all experiments consist of 0.01 mm thick films of naphthalene sandwiched between glass plates (Fig. 1). The sample is produced by melting a few crystals of naphthalene between two glass plates under compression, and quenching the melt by using either a water or silicone oil circulation system built into the deformation apparatus. A skeletal intergrowth of naphthalene crystals grows from the melt after an undercooling of 10–15°C and is dominated by a simple array of two parallel elongate crystal sets with alternating width and lattice orientations. Growth of the aggregate is controlled by the fibre-like, herein called skeletal (S), crystals (Fig. 1a). Grain boundaries coincide with a common crystallographic direction, always lying in (001) and close to [b] in both sets of crystals (Fig. 2). The lattice rotation angle between adjacent crystal sets is usually 30°, but with rare values ranging from 10° to 40°.

The S crystals always have (001) and associated cleavage inclined to the constraining glass windows and first-order interference colours (grey to orange) between crossed nicols. The interskeletal (I) crystals have (001) subparallel to the glass and contain subgrains with misorientations of 1–3°, showing third-order interference colours (green to red). Subgrains are prominent because of naphthalene's high birefringence (Table 1). In the samples used in this investigation, average [b] axis orientation common in I and S crystals is sub-parallel to the constraining glasses and the grain boundaries produced by crystal growth (Fig. 2b). Departure from this situation is limited (Figs. 2c & d) and misorientation between the grain boundaries and [b] axes never exceeds 30°.

Kinematic constraints

Translation of the upper glass relative to the fixed lower glass (Fig. 1b) induces a bulk simple shear expressed (Fig. 3) by the transformation of co-ordinates of material points in the reference axes (X_1, X_2). The sample has to remain unstrained in the third direction perpendicular to the deformation plane (plane strain) as the thickness of the film is kept approximately constant by the glass windows. In the deformed samples described here, the skeletal intergrowths generally extend across the sample with the ends of the crystals locked by the area of frosted glass (Fig. 1). The section of the crystal that overlaps the frosted area remains undeformed and deformation is confined to the intervening central area (Fig. 1). Therefore, the inner margins of the frosted areas behave as coherent boundaries (Cobbold *et al.* 1984, Means & Jessell 1986) if there is no lateral fracturing or de-coupling of the crystals from the frosted area (Fig. 3) and grain boundary sliding is impossible along the sample margins. To fulfil these conditions and keep the boundaries undistorted, the local deformation gradient tensor **D** expressed in the references axis (X_1, X_2) should have:

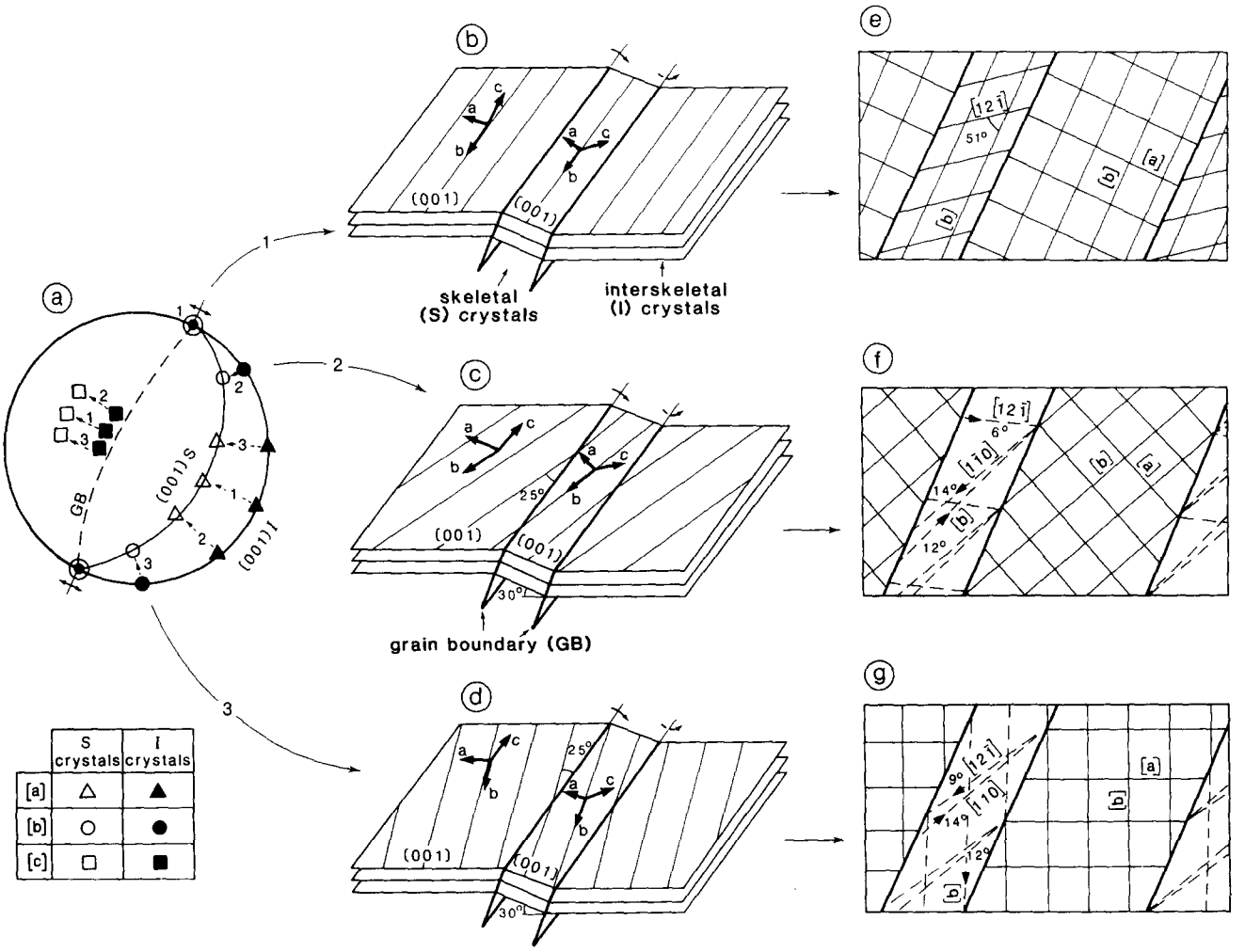

Fig. 2. Typical sample configurations (1–3) and the relationship to crystallographic orientation of skeletal (S) and interskeletal (I) naphthalene crystals. (a) Lower-hemisphere stereographic projection (equal angle) in the plane of the sample. (1) is average case with a common [b] axis parallel to the grain boundaries (GB) in the S and I crystals, (2) and (3) illustrate the extreme departure of [b] from the GB direction. All the intermediate situations between (1) and (2), or (1) and (3) are possible. From 42 U-stage measurements. (b)–(d) Sketches illustrating the alternate tilting of (001) in the I and S crystals about a common crystallographic direction in (001) oscillating around [b]. (e)–(g) Calculated orientation of the potential slip directions for the three typical samples. Projections in the constraining glass window plane. Unbroken lines correspond to slip directions parallel to the glass; dashed lines are inclined to slip directions with dip value and direction.

$$\mathbf{D}_{11} = 1$$
$$\mathbf{D}_{21} = 0$$

at the sample margin. In this situation, there are two classes of progressive deformation that need to be considered:

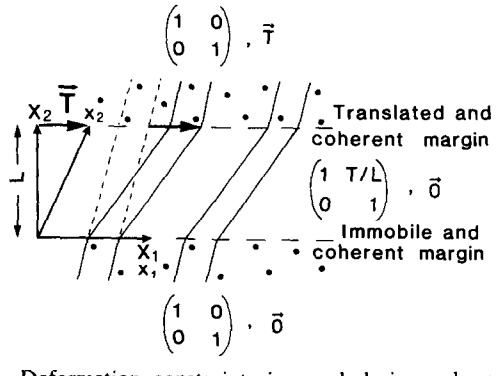

Fig. 3. Deformation constraints imposed during a homogeneous deformation of an I/S crystal aggregate between glass frosted areas (dotted). Finite deformation of each domain is defined by the deformation gradient tensor, plus the translation vector.

(1) homogeneous and non-spinning simple shear (Means *et al.* 1980) parallel to X_1 in each crystal;

(2) bulk simple shear parallel to X_1 on the scale of the sample with a heterogeneous distribution of the deformation within the sample. As a consequence of the rigid boundary conditions, deformation should (a) tend laterally to non-spinning simple shears parallel to X_1, or (b) cancel in contact with the margins.

Slip systems

The eight slip systems observed in naphthalene and in the closely related anthracene (Table 1) can be subdivided into easy basal systems with slip on (001) along [b] and ⟨110⟩. The hard non-basal slip systems exist on (100), (010), {111} along [a], [b], [c] and also ⟨1$\bar{2}$1⟩. However, the crystallographic orientation of the crystals with respect to the constraining glass plates favours those slip systems with the slip direction subparallel to the glass and slip plane oblique to the glass. The number of potentially activated slip directions would therefore

be limited to two or three in each crystal, mostly non-basal systems (Fig. 2), and depends on the *I* or *S* crystal type.

In the *I* crystals, the perpendicular [*b*] (100) and [*a*] (010) are the active slip systems. In the *S* crystals with an average crystallographic attitude (Figs. 2b & e) the slip systems are [*b*] in (001) or (100) and [12$\bar{1}$] (1$\bar{1}$1). However, the situation is less favourable for a general slip (Figs. 2f & g), in which the slip direction is inclined to the glass: −9° to +6° for [12$\bar{1}$], −12° to +12° for [*b*], and 14° minimum for [110] or [1$\bar{1}$0].

RESULTS

The skeletal intergrowths of *S* and *I* crystals that generally extend across a sample have varying orientations with respect to the frosted areas. The contrasting deformation induced microstructures that develop during the imposed shearing depend on the initial orientation of the intergrowths and the [*b*] axis with respect to the shear direction, expressed by the angle ρ (Fig. 4). Two prominent fields (Fig. 4) of contrasting deformation are identified that correspond to (1) *shortening* where the [*b*] axis is oriented $0° < \rho < 90°$ and the deformation is dominated by kinking, and (2) *stretching* where the [*b*] axis is oriented $90° < \rho < 180°$ and rapid migration of the *I/S* boundaries produces a necking of the *S* crystals. The initiation and progressive development of these features occur within a limited range of average finite shear strain (γ) typically 0.2–0.5. Where γ exceeds these critical values the shearing tends to localize into zones that are dominated by recrystallization. Described below are examples of the early microstructural evolution of typical experiments (Figs. 5 and 6) prior to the onset of extensive recrystallization.

[b] *axis inclined at high angle to shortening direction*

The progressive deformation of aggregates with *S* crystals and [*b*] axes that are initially oriented at a high angle to the shear direction, $\rho > 60°$, are illustrated in Fig. 5. After a gentle and continuous bending of the crystals, deformation is confined to kinks located adjacent to one frosted glass margin. The kinks nucleate (Fig. 5a) as narrow discontinuous kink bands (KBs) arranged in an en échelon array and subperpendicular to the *I/S* boundaries. Increasing deformation (Figs. 5b & c) is accommodated by kinks where the naphthalene lattice progressively rotates according to the sense of shearing and where the kink angle can be defined by the rotation of *I/S* boundaries across the kink band boundaries (KBBs). KBs become optically more prominent as the [*b*] = β direction approaches a vertical extinction position (see Table 1 for optical properties). As required in kink band models (Starkey 1968, Weiss 1980) the KBBs are coherent and, on the optical scale used here, do not offset the *I/S* boundaries. For each individual KB, KBBs migrate while rotating progressively towards the shearing direction and keep a symmetric attitude approximately bisecting the kink angle. The en échelon KBs tend to coalesce along their length and transform into a unique KB parallel to the shearing direction (Fig. 5c). Small steps in the KB are developed where the frosted area is irregular or gently curved (arrow in Fig. 5c) and are associated with narrow offset KBs connected by small extensional fractures.

With increasing shear (Figs. 5d–j) there is a marked widening of the KB perpendicular to its boundaries. This is not due to a continuous lateral migration of the KBBs, but proceeds (Figs. 5c–i) by the periodic formation of new KBBs that lie outboard in the undeformed naphthalene. A new KBB (KBB_n) typically nucleates as a planar boundary subperpendicular to [*b*] (arrow in Fig. 5c) and delimits the kink as long as its orientation rotates towards the shear direction by rotation migration (Figs. 5c–g). When the boundary gets parallel to the shear direction, a new KBB (KBB_{n+1}) forms outboard (arrow in Fig. 5c) and KBB_n is hence enclosed into the kink. Naphthalene flanking KBB_n progressively unfolds due to a higher rate of lattice rotation in the outer limb and KBB_n progressively disappears (Figs. 5g–i). At the same time, its rotation migration slows down beyond the shear direction and its shape becomes serrated. It persists in the enlarged kink in the form of lozenge shaped subgrains.

The stages in the progressive widening of a KB are summarized in Fig. 7. The evolution of these complex kinks represents a heterogeneous deformation where the inner and hence older KBs become progressively more dormant. Most of the imposed shearing is accommodated by the two outer KBs. Deformation therefore tends to localize along the margin of the widening kink and moves across the sample perpendicular to the shear direction.

Recrystallization (Fig. 5f) is superimposed on the KBs, but is an experimental artefact; small new grains develop with asperities fringing the frosted area (arrow in Fig. 5f) and do not appear in every experiment of this type. Asperities plough the naphthalene film during their translation and induce a trail of recrystallization behind them. When the translation is sufficient, the different trails connect in a recrystallized band that

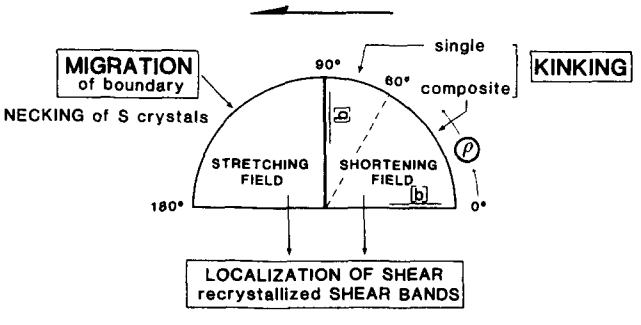

Fig. 4. The two-dimensional fields of shortening (0–90°) and stretching (90–180°) during a sinistral simple shear of elongate grain aggregates inclined at an angle ρ to the margin of the frosted areas. The microstructural evolution in the *I/S* crystal intergrowths is a function of the obliquity angle ρ of the crystal length and of their [*b*] axis to the frosted areas.

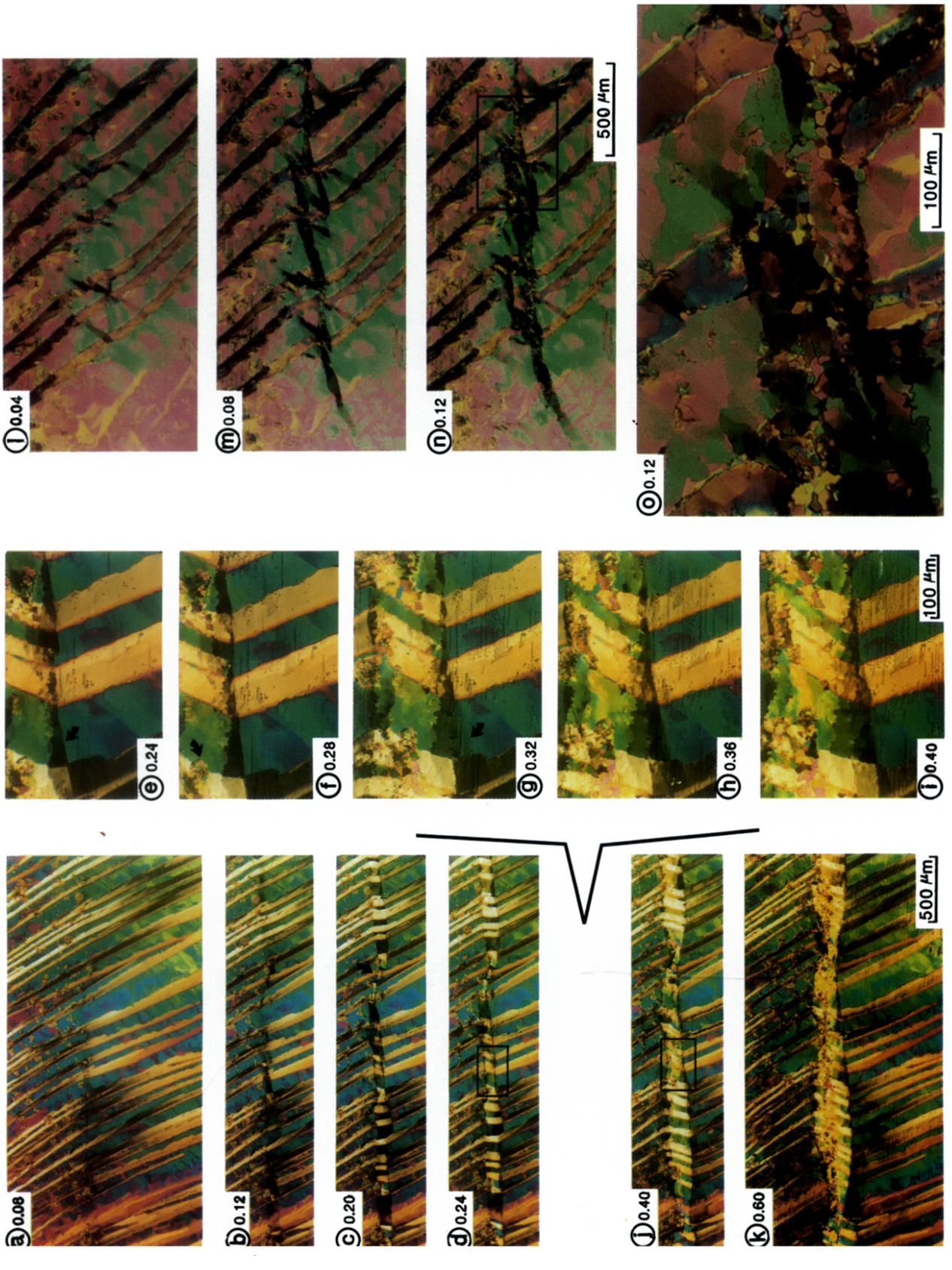

Fig. 5. Typical progressive shearing and microstructure evolution in naphthalene aggregates with [b] axis in shortening direction. The average shear strain (γ) is shown on the left-hand corner of the micrograph. (a)–(k) Experiment No. 8, $\rho = 65°$, temperature = 47°C. (l)–(o) Experiment No. 16, $\rho = 40°$, temperture = 61°C.

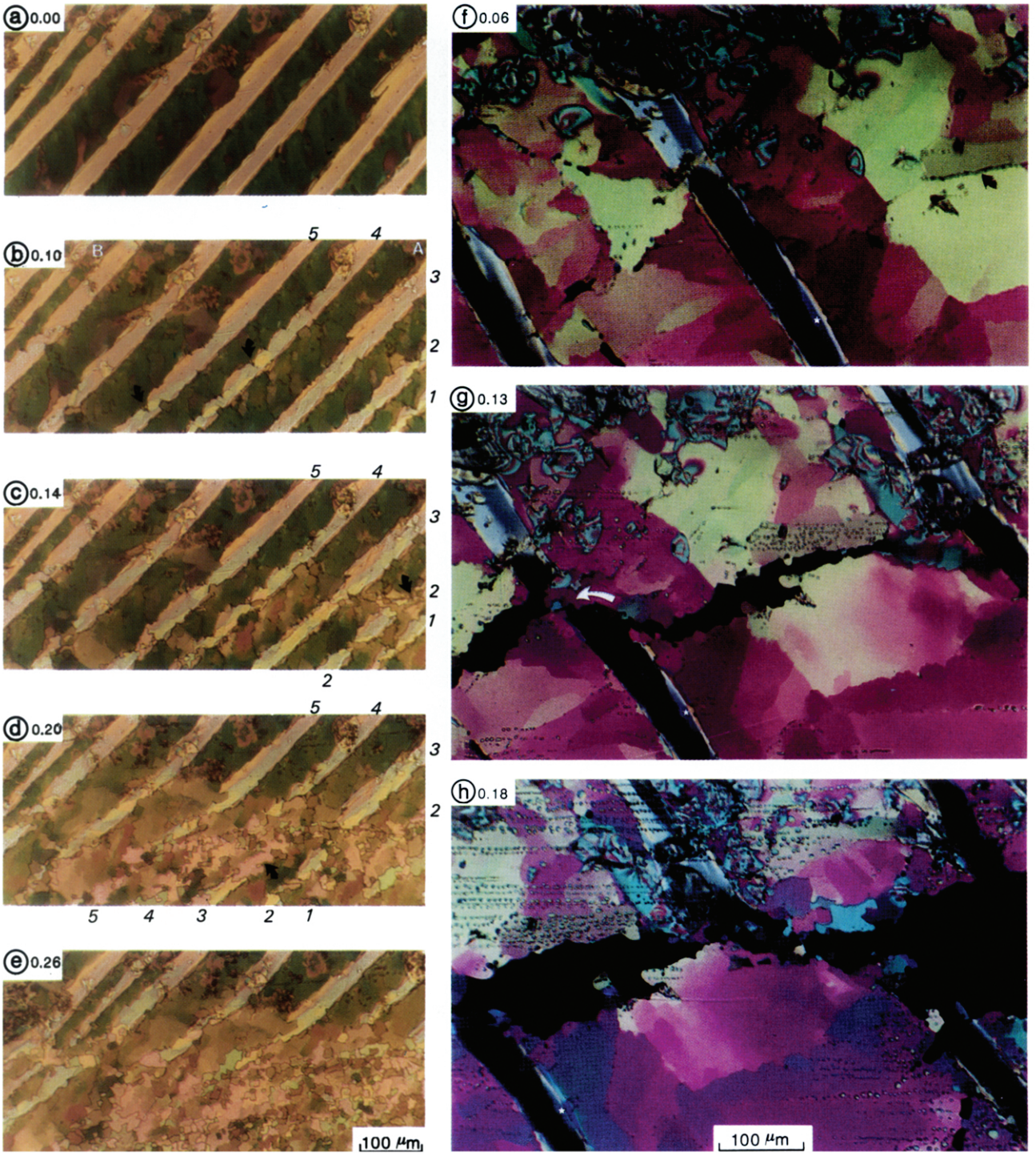

Fig. 6. Typical progressive shearing and microstructure evolution in naphthalene aggregates with [b] axis in stretching direction. The average shear strain γ is shown on the left-hand corner of the micrograph. (a)–(c) Experiment No. 20, ρ = 130°, temperature = 61°C. (f)–(h) Experiment No. 30, ρ = 120°, temperature = 61°C.

records part of the imposed simple shear. The majority of the deformation is accommodated by the kink that keeps on progressively widening (Fig. 5k).

[b] *axis inclined less than 60° to shortening direction*

In situations where the initial inclination (ρ) of the *S* crystals is less than 60° (Fig. 4) the deformation and lattice rotation that accompanies the shortening is not confined to a unique kink band but occurs as a composite kink set (Figs. 5l–n). The KBBs that nucleate subperpendicular to the [*b*] axis early in the experiment (Fig. 5l) define an array of parallel KBs with alternating widths and senses of rotation. The wider bands or limbs of the KB rotate according to the sense of shearing, with the opposite shear sense in the narrower limbs. This system decays as soon as the [*b*] axis in the large limbs becomes oriented subperpendicular to the imposed shear direction (Fig. 5m). Secondary internal KBBs are then nucleated again subperpendicular to the rotated [*b*] direction in the form of long continuous KBs that subparallel the shear direction. The latter KBs intersect the tilted narrow limbs of the early kink folds at complex 'nodes' where recrystallization is initiated by migration of the high-angle boundaries (KBBs and *I/S* boundaries). These processes will be described more precisely in the following section. Recrystallization spreads along the secondary KBs (Figs. 5n & o) and creates a recrystallized band that parallels the shear direction and accommodates the imposed shear.

[b] *axis in stretching direction*

The behaviour of the sample during shearing is strikingly different when crystals and the common [*b*] axis are oriented along a stretching direction (Fig. 4). The microstructural evolution (Figs. 6a–e) is dominated by a marked migration of the *I/S* boundaries leading to the formation of a recrystallized shear band. These boundary adjustments are initiated during the first increments of deformation and occur in the zone of maximum bending. Along the length of an *I/S* crystal interface (Fig. 6b) boundaries migrate with *I* crystals consuming *S* crystals, the latter becoming narrower (Figs. 6a & b). Further migration is localized (Figs. 6b & c) to produce bulges, with *I* crystals penetrating *S* crystals, that enlarge into lobes with increasing deformation, until the *S* crystals are 'dissected' (Urai *et al.* 1986) or 'boudinaged' (Fig. 6c). The direction of grain boundary migration from A to B (Fig. 6b) is variable in different experiments and cannot be related to the sense of shearing or curvature of crystals.

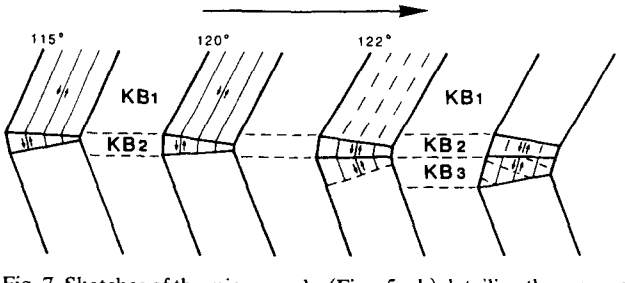

Fig. 7. Sketches of the micrographs (Figs. 5e–h) detailing the progressive widening of the kink band by successive nucleation of new onboard kink band boundaries.

Further shear is localized, as shown by the displacement of numbered *S* crystals (Figs. 6c & d). A high shear strain zone initiates along a sample margin, where the first *S* crystal is necked by bulging (arrow in Fig. 6c). Most of the shear is accommodated in a very local area close to the newly created grain boundaries that cross-cut the *S* crystal and this suggests that these new grain boundaries are incoherent and are affected by sliding (arrow in Fig. 6c). Recrystallization develops at the tip of the new grain boundary and a recrystallized grain structure is then propagated longitudinally through the sample parallel to the shear direction, together with the high shear strain zone (Fig. 6d).

The recrystallization processes involve (1) bulging of the original *I/S* boundaries, and (2) progressive misorientation followed by bulging of the primary growth sub-grain boundaries producing serrated boundaries within the *I* crystals. The first new grains are created by a bulging, i.e. a small lobe created at the boundary of the *I/S* interface migrates into the *S* crystal (Fig. 6), with a progressive misorientation of the lobe with respect to the host crystal to develop a sub-grain (Means 1981, Urai *et al.* 1986). This gives a transient structure that mimics the original *I/S* structure with *S* crystals being replaced by elongated sub-grains with *I* type lattice orientation (arrow in Fig. 6d). However, the new grain boundaries and the misorienting sub-grain boundaries related to the bulges start migrating, become serrated and create secondary bulges. The latter evolve into small new grains that overprint and destroy the original *I/S* structure (Fig. 6e).

Migration of the boundaries is crucial in these experiments and is dramatically illustrated if *S* crystals and *I/S* boundaries have greater spacings (Figs. 6f–h). In the experiment shown in Fig. 6(f), where the spacing of *S* crystals is approximately 6 times greater than the other samples, cracks nucleate during the first incremental deformation in *I* crystals along the primary growth subgrain boundaries oriented in the shortening direction (arrow in Fig. 6f). Propagation of these cracks is restricted within *I* crystals, as bulging of the *I/S* boundaries occurs at their tips (Fig. 8) and forms new cross-cutting grain boundaries that localize the shear (arrow in Fig. 6g). Imposed shearing is then accommodated by displacement on the dilating and shearing fractures contained in *I* crystals, and this is then transmitted by sliding along the new and incoherent grain boundary across *S* crystals (Fig. 6g). As previously described, these primary bulges evolve into new grains, that in turn form secondary bulges, until the area around the initial *I/S* boundaries is recrystallized (Fig. 6h). It gives a brittle–ductile shear band along which shear fractures and local recrystallization mosaics alternate.

Ductility of the samples is correlated to *S* crystals and *I/S* boundary spacing. When spacing is high (several

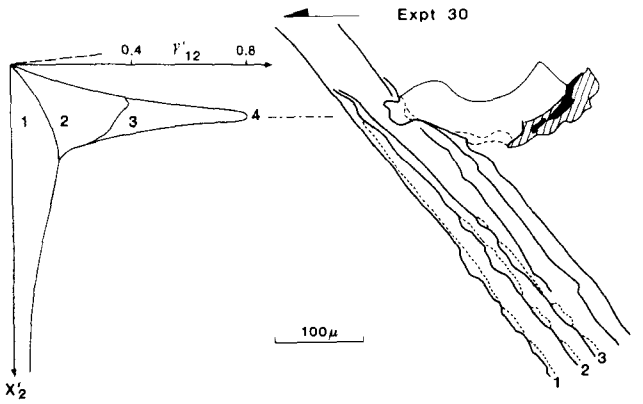

Fig. 8. Sketch illustrating the bulging of *I/S* boundaries (experiment No. 30) taken from data recorded on 16 mm film during the deformation. Measurements of displacements of the *I/S* boundary where grain boundary migration is limited, and of small impurities included in the *S* crystal show a progressive localization of shear strain (γ) where the bulge occurs.

hundreds of microns), behaviour of the sample is brittle; on the contrary, imposed shear can be accommodated in ductile shear bands if the array of original boundaries is dense enough (spacing $\leq$100 μm). It strongly suggests that ductility of samples oriented in the stretching field is a function of the density of high-angle grain boundaries able to migrate and to slide.

Recrystallized shear bands

Localization of shear in shear bands occurs after the first stage of kinking or necking. The shear bands are typically 50–400 μm wide and contain isometric to slightly elongated recrystallized grains usually 10–40 μm in diameter. The size of new grains is fairly constant over a wide range of temperatures below the melting temperature (45–75°C), but increases sharply in experiments formed around the melting temperature (80°C) with a melt fraction visible in some cases. In the high-temperature experiments, grain size is heterogeneous and ranges from 30 to 130 μm, with some ribbon-shaped crystals reaching several hundred microns in length.

Lattice preferred orientations of [*b*] axes developed in the shear bands (Fig. 9) always show a single point maximum parallel to the shear direction; [*c*] and [*a*] axes lie in a plane perpendicular to the shear direction. The plunge of [*a*], [*b*] and [*c*] axes with respect to the constraining glasses remains statistically unchanged to that of the undeformed *I* and *S* crystals. Lattice axes rotate on small circles (Fig. 9) during deformation with a common rotation axis perpendicular to the constraining glasses.

Migration of the grain boundaries is extremely active in the shear bands and the grain mosaic is hardly recognizable after a few minutes of deformation. Serial fabric measurements have been recorded in several experiments by deforming samples for 2 min periods and stopping experiments for *U*-stage measurements. Development of the lattice fabric is produced by a selection of grains in the recrystallized shear bands, with [*b*] axes parallel to the shear direction. Differently oriented grains are consumed by grain boundary migration, which is the major process contributing to the development of this lattice fabric. This is similar to the processes described by Bouchez & Duval (1982) in ice and modelled by Jessell (1986) in octachloropropane.

DISCUSSION

Mechanical anisotropy

An extreme anisotropy is revealed in the melt-grown naphthalene samples when sheared in specific directions. This anisotropy can be described as a function of angle ρ that expresses the orientation of the [*b*] axis and the *S* fibres relative to the shear direction:

(1) when [*b*] is oriented in the shortening direction, crystals kink with KBBs nucleating subperpendicular to [*b*] and migrating in order to keep a symmetrical attitude with respect to [*b*];

(2) when [*b*] is oriented in the stretching direction, *S* crystals undergo 'boudinage' due to the migration of *I/S* boundaries, and *I* crystals fracture if *I/S* boundary spacing is large.

Macroscopic analysis of these contrasting structures, i.e. kinking vs boudinage and extension fracturing, are reminiscent of tectonic processes observed in finely laminated rocks where deformation is achieved by sliding along lamina surfaces (foliation, bedding) that are considered inextendible. Kinks or concentric folds

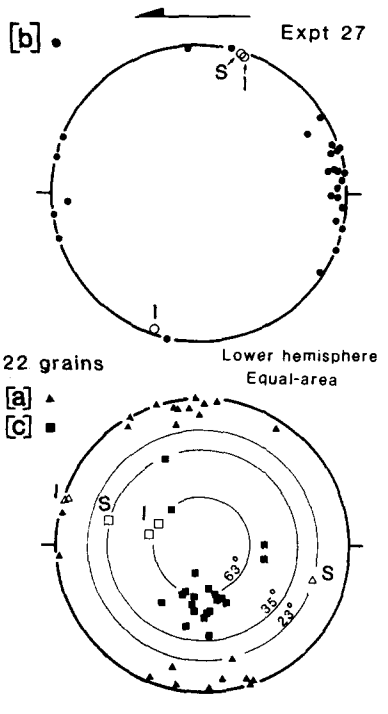

Fig. 9. Lattice preferred orientations measured in recrystallized shear bands with U-stage [*b*] axis stereogram (upper) and [*a*] and [*c*] axis stereogram (lower). Open symbols correspond to [*a*], [*b*] and [*c*] orientations in undeformed *I* and *S* crystals.

develop by sliding along the bedding planes during the buckling of the layers, in more or less stratified formations subjected to shortening; when stretched, deformation is unstable and localizes in fractures and boudin necks of more competent layers (Ramsay 1967).

Dominant [b] *slip*

An analogy for penetrative stratification at the crystal lattice scale would involve intracrystalline slip with a common orientation in *I* and *S* crystals. Such a possibility, involving [*b*] slip, has already been considered when reviewing slip systems in deformed monocrystals and selecting slip directions close to the imposed deformation plane in skeletal naphthalene aggregates. [*b*] is a major slip direction in naphthalene and operates in (001) under low stress and in (100) for higher stresses (Table 1).

The geometry and kinematics of the KBBs agree with dominant [*b*] slip. KBBs nucleate subperpendicular to [*b*] and behave like tilt walls composed of edge dislocations with Burgers vector [*b*], in accordance with McLaren & Etheridge's model (1980). The tilt axis is required to be perpendicular to the moving glass windows in order to get plane deformation, and it would be geometrically achieved by mixing [*b*] dislocations generated in (001) and (100), or by climbing of [*b*] dislocations in either of these planes.

KBs migrate when the kink angle increases to maintain a near-symmetrical orientation of [*b*] on both sides of the KBBs. This satisfies the angular coherency conditions at the KBBs for a dominant [*b*] slip, required by (1) KB kinematic models in laminated material (Weiss 1980, Cobbold *et al.* 1984), and by (2) KB crystallographic models (Starkey 1968, Baronnet & Olives 1983) for which the KBB is a plane of lattice coincidence of the two crystal domains. Because of the monoclinic symmetry, exact coincidence can be realized at symmetric KBBs with any [h0l] rotation axes, one of which is also normal to the glass windows in *I* crystals, as well as in *S* fibres for samples with an average crystallographic setting (Figs. 2b & c) that meet the plane deformation condition.

The lattice fabric (Fig. 9) in recrystallized shear bands of naphthalene further supports [*b*] as the dominant slip direction. The point-maximum in the [*b*] axis stereogram is centred on the shear direction. This is a common pattern of lattice preferred orientation in many naturally sheared mineral aggregates. A good example is provided by quartz in which ⟨*a*⟩ or [*c*] slip is dominant depending on the physical conditions. A switch from ⟨*a*⟩ to [*c*] slip does not alter the pattern of the lattice preferred orientation diagram but the point-maximum close to the shear direction is either drawn by ⟨*a*⟩ or [*c*] axes, respectively (Blumenfeld *et al.* 1986). Numerical simulations of fabrics also reproduce this preferred orientation of the slip direction, provided that the single slip hypothesis is applied (see discussion by Bouchez *et al.* 1983).

Heterogeneity and localization of the deformation

All the experiments are characterized by a highly heterogeneous distribution of deformation within samples and a localization of deformation after limited shear. A dominant [*b*] slip is not sufficient to homogeneously accommodate an imposed deformation, the minimum number of slip directions being two in a plane strain deformation (Taylor 1938). The resulting deformation heterogeneity within *I* and *S* crystals requires the formation of either:

(1) *coherent* boundaries, represented by low-angle sub-grain boundaries or KBBs, defining domains where deformation is homogeneous, but differs from one domain to another; or

(2) *incoherent* boundaries along which sliding occurs. These must be high-angle boundaries and result from misorientation of sub-grain boundaries or migration of high-angle *I*/*S* boundaries. Sliding along high-angle boundaries probably accompanies the recrystallization of naphthalene as it is transformed into a mosaic of new grains and destroys the original growth structure (Figs. 6c & d). This type of boundary is associated with a loss of continuity at the lattice scale, but can retain continuity at sample scale. If an obvious discontinuity develops, the incoherent boundary can grade into a shear fracture.

Coherent boundary conditions at the margins of naphthalene samples are realized by localization of deformation and accommodation of imposed shear in deformation bands bounded laterally to undeformed naphthalene. Dominated by a single [*b*] intracrystalline slip, the deformation band has to be an *S*-type simple shear perturbation as described by Cobbold (1977) in order to maintain continuity with the undeformed portion of the sample. This *S*-type includes (1) shear bands where deformation is a non-spinning simple shear and whose orientation is stationary with increasing deformation, or (2) kink bands (simple or composite) where deformation is a spinning simple shear and KBBs migrate.

Shear bands with coherent boundaries at the lattice scale would correspond to slip bands parallel to [*b*]. These shear bands are unlikely to appear as they are unable to accommodate the imposed simple shears unless the [*b*] axis of the sample parallels the frosted areas. Only shear bands associated with recrystallization within *I*/*S* crystals, and formation of high-angle boundaries where sliding is possible, are able to accommodate the imposed shear parallel to X_1.

Accommodation of deformation by kinks

Kinking is a prominent accommodation process that precedes recrystallization and this is demonstrated in experiments where [*b*] is oriented in the shortening direction. The imposed simple shear can be accommodated by single or composite kink sets (Figs. 5l–n) and is discussed with reference to the kink band model of Weiss (1980) and the general kink model of Cobbold & Gapais (1986).

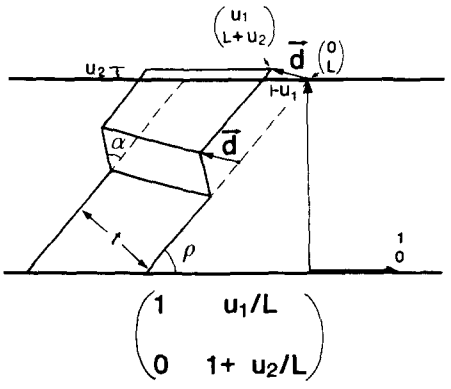

Fig. 10. Bulk finite deformation in a material cross-cut by a Weiss (1980) mode 1 kink band ρ; orientation of the single slip with respect to the axis system; L, width of the sample along the ordinate axis; t, width of the sample perpendicular to the slip line; α, kink angle expressing the rotation angle of the slip line in the kink band; d, displacement of a point of the sample top, with components U_1 and U_2.

(a) *Single kink band.* Single KBs with rotating KBBs are observed in experiments with $60° < \rho < 90°$ (Figs. 5a–c). They correspond to Weiss' (1980) mode 1 (Fig. 10) where the kink angle α increases and KBBs rotate with increasing deformation. In the Cobbold & Gapais (1986) model, the kinks would involve deformation mode 1 (bulk elongation parallel to the average direction of the inextendible slip line, by buckling) and mode 3 (bulk shearing parallel to the same average direction). Bulk finite deformation due to kinking is expressed by the gradient deformation tensor shown in Fig. 10 and differs from the imposed simple shear parallel to X_1 if U_2/L is not $=0$. For different values of obliquity ρ it is possible to characterize the finite elongation U_2/L perpendicular to X_1 vs finite shear U_1/L parallel to X_1 (Fig. 11). The imposed simple shear is only accommodated where KBBs parallel X_1, for $\alpha = 180° - 2\rho$. A compensating shortening or stretching is otherwise needed perpendicular to X_1 in order to yield the imposed simple shear. For α values ranging from 60° to 90° the required shortening is limited to a fraction of a percent during the initial activity of the KB until KBBs parallel the shear direction. The initial shortening is probably accommodated by elastic strain and/or destruction of initial porosity.

(b) *Composite kinks.* A single mode 1 KB cannot function alone if substantial shortening or stretching is needed perpendicular to X_1 (Fig. 11). Two specific cases were noted in the current set of experiments. **Case 1** for $60° < \rho < 90°$ when $\alpha > 180° - 2\rho$ (i.e. KBB rotate beyond X_1, Figs. 5d–k) and **Case 2** for $\rho < 60°$ from the beginning of deformation (Figs. 5l–o).

Further shearing in **Case 1** (Figs. 5d–k) could be simply accommodated if the mode 1 KB transformed into a mode 2 KB (Weiss 1980) when $\alpha \leq 180° - 2\rho$. KBs parallel to X_1 would widen by lateral migration of the KBBs and accommodate increments of simple shear by transformation of the slipline orientation and its instantaneous incorporation in the KB (deformation mode 2 of Cobbold & Gapais 1986). It is clear from Figs. 5(d)–(k) and other experiments that this process is not active, at least not alone, in these deformed samples. Resistance to lateral migration of the KBB should be greater than resistance to formation of a new KBB and widening occurs by formation of outboard KBBs (Figs. 5c–i). The role of these outboard KBs to accommodate the imposed simple shear can be broadly realized in noticing that finite shortening (perpendicular to X_1) provided by the old KB ($\alpha > 50°$ for $\rho = 65°$) can be balanced by finite stretching perpendicular to X_1 and produced by the newly formed outboard KB ($0 < \alpha < 50°$ for $\rho = 65°$). When an outboard KBB reaches the X_1 direction, the KB cannot provide the compensating shortening and a

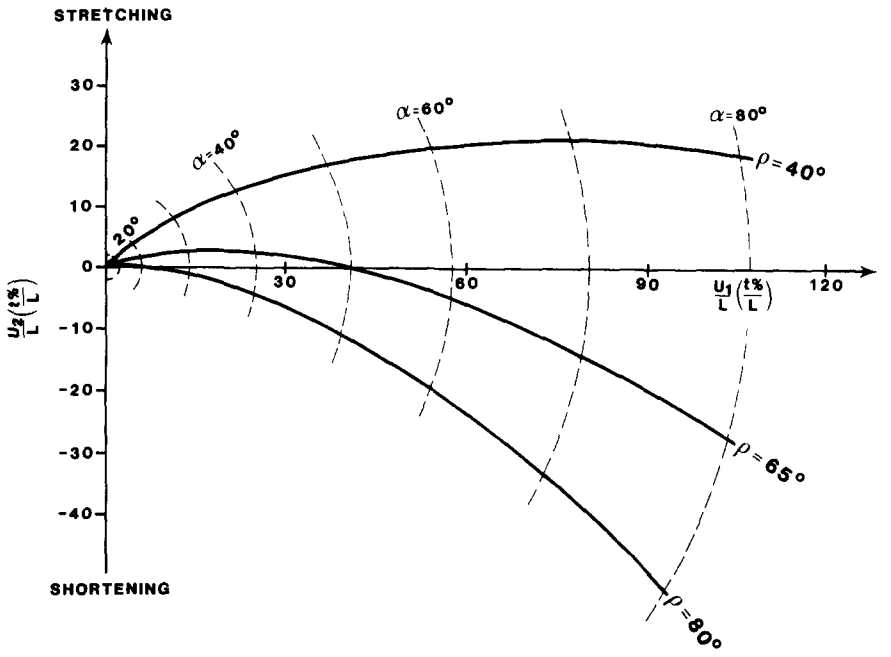

Fig. 11. Finite elongation U_2/L perpendicular to X_1 vs finite shear U_1/L parallel to X_1 for different values of the kink angle α and of the obliquity ρ of the slip line to X_1. In the case of Fig. 9, t/L is in the order of 10^{-1} in these naphthalene samples.

new accommodation system forms with the nucleation of a new outboard KBB.

Case 2 with $\rho < 60°$ provides an example where composite kinking is required from the onset of deformation and is an illustration of Cobbold & Gapais' (1986) model. Using a two-dimensional kink-type structure composed of parallel and coherent bands of alternating widths and single slip orientations, Cobbold & Gapais (1986) showed that two differently oriented domains with migrating boundaries produce two independent slips on the sample scale. This is a minimum requirement to accommodate any bulk deformation and is analogous to the Von Mises criterion applied to a heterogeneous deformation. The situation where the average slip direction is oriented in shortening in an imposed bulk simple shear involves deformation modes 1 and 2, or 1 and 3 (Cobbold & Gapais, 1986), the latter combination being of special interest in the experiments as mode 2 seems to be little active or inactive. However, the system ceases to be active when new KBBs parallel to X_1 nucleate within domains where [*b*] rotates perpendicular to X_1 (Figs. 5l & m). As shown in Fig. 11, such a simple shear can accommodate an increment of simple shear, but further shearing requires the recrystallization of naphthalene and the creation of high angle boundaries (Figs. 5n & o).

Necking of S *crystals and migration of grain boundaries*

In Cobbold & Gapais' (1986) model, stretching parallel to the average slip direction can be achieved by opening the kink angle of a pre-existing kink. If the [*b*] axis of undeformed naphthalene crystals is oriented in a stretching direction, no deformation mode involving a dominant [*b*] slip is able to accommodate stretching parallel to the slip direction. Deformation is unstable after very small increments of shear (Fig. 4) with nucleation of extension fractures perpendicular to crystal length and necking of *S* crystals. The latter occurs after plastic yielding of the crystals, together with sub-grain boundary development, and is a manifestation of plastic deformation instabilities very much like geological flow associated with boudinage (Smith 1975). The general instability model at constant strain rate (Poirier 1980) relates the concentration of strain and the occurrence of a local process that allows further straining at lower applied stress. Consequently, necking involves an overall softening of the sample, which cannot be achieved without a rheological contrast. Necked *S* crystals need to be harder or 'more competent' than *I* crystals, i.e. have a higher strain rate sensitivity of stress and/or a higher strain hardening coefficient. The difference in rheology between pure naphthalene crystals can only be produced from a mechanical anisotropy and this can be related to a difference in slip system orientation with respect to shear geometry. In these experiments, as soon as the sample departs from the average crystallographic setting (Fig. 2c), all the known slip directions in *S* crystals are oblique with respect to the constraining glasses (Figs. 2f & g). A three-dimensional deformation occurs in the *S* crystals and can be observed as a change of interference colours in the vicinity of the necks (arrows in Fig. 6b) where sub-grains rotate about an axis oblique to the glasses and/or vary slightly in thicknesses.

Only considering the strain component of an imposed deformation, five slip systems would be required to accommodate any finite plane strain in the *S* crystals, and this would be reduced to two in the case where slip directions parallel the strain plane as in *I* crystals. This suggests that deforming *S* crystals involve more slip systems and, among them, hard slips with high resolved stress and/or badly oriented slip planes requiring high applied stress.

Further modelling of the accommodation of imposed deformation by three-dimensional heterogeneous deformation in *S* crystals should take the following parameters into account (1) the eight possible slip systems, (2) the conditions at the sample limits in three dimensions, including the already stated ones in the glass plane along frosted areas and additional ones in the third dimension to describe the contact of crystals against the glasses, and (3) coherency conditions at the crystal internal boundaries. A qualitative examination of the three-dimensional problem is unable to state if a solution exists. If not, any increment of imposed deformation requires an increment of load-supported elastic deformation to complement the plastic deformation with a subsequent increase of the applied stress. Activation of unfavourable slips, extra hardening due to multiplication of dislocations and, possibly, an increasing load-supported elastic deformation, are likely to increase strain rate sensitivity of the stress and strain hardening coefficient of *S* crystals relative to *I* crystals, creating the rheological contrast.

The actual process of 'boudinage' involves migration of boundaries through the crystal lattice and replacement of *S*-type by *I*-type orientation. Driving force for synkinematic grain boundary migration is mainly related to a decrease of elastic distortional energy (Urai *et al.* 1986) with the migration direction going up the energy gradient. A model for grain boundary migration in single phase polycrystals is provided by the experiments of Jessell (1986) and is also applicable to the present set of experiments. The elastic energy of the octachloropropane grains (Jessell 1986) can be correlated to their basal slip plane orientation with respect to the applied stress. Grains poorly oriented for easy glide will be associated with high elastic energies and will be consumed by adjacent grains which have easy glide orientations and lower elastic energy. Similarly, a high level of elastic energy is likely to occur in *S* crystals. The load-supported elastic energy, due to the high applied stress required (1) to activate unfavourble slip in *S* crystals, and (2) possibly complement plastic deformation with significant elastic deformation, is likely to be prominent in the first increments of deformation and to initiate an extensive migration of the *I*/*S* boundaries in the zone of crystal bending. It is probably over-ridden by intragranular defect elastic energy when dislocations multi-

ply to further deform *S* crystals. A very heterogeneous distribution of elastic energy is therefore produced along the *S* crystals, with recovery processes producing subgrain boundaries associated with high and local dislocation density at bulging *I/S* boundaries.

Consumption of hard *S* crystals by migration of grain boundaries is a strain softening process of the structural type (Poirier 1980) and creates a flow instability as soon as it localizes by bulging. A second softening process takes over when *S* crystals are cross-cut by the high-angle boundaries of bulges. Sliding can then occur along these boundaries sub-parallel to the shear direction and destroy the initial kinematic constraints generated by sample growth. New grains that nucleate from bulges in *S* crystals form the nucleus for development of recrystallized shear bands that accommodate further imposed shear by deformation processes usually associated with a polycrystalline aggregate (Wilson 1986).

The existence of high-angle grain boundaries and grain boundary migration are the key factors for a ductile accommodation of the imposed shear when [*b*] is oriented in the stretching field (Fig. 4). This is well illustrated by alternating ductile recrystallized mosaics around *I/S* boundaries and fractures away from them (Fig. 6). When high-angle boundaries act as loci for sliding, this greatly diversifies the processes helping intracrystalline slips to accommodate the imposed deformation. The migration of high-angle boundaries is a ductility-enhancing factor and is achieved by increasing the length of high-angle boundary. The role of grain boundaries also accounts for the very high homologous temperatures of the brittle–ductile transition in these experiments and is likely to relate to the very important thermoactivation of the velocity for grain boundary migration (Urai *et al.* 1986).

CONCLUSION

These experiments demonstrate that naphthalene is a valuable rock analogue that replicates microstructural changes associated with the deformational behaviour of a highly anisotropic material with a single dominant slip system. By imposing strict kinematic constraints, through the application of rigid contacts to the crystal, a number of accommodation processes are needed to complement intracrystalline slip in the deforming anisotropic crystal aggregate. These processes do not co-exist in the same experiment and the orientation of the dominant slip system is critical for the selection of the major accommodation process. The experiments illustrate the importance of two dominant processes.

(1) *Kinking* which is the basis of the kinematic models of Cobbold & Gapais (1986) and occurs when [*b*] is oriented in the shortening field. The crystal accommodates the imposed simple shear by intragranular kinking and avoids recrystallization at low strain, especially if ρ angle is in excess of 60°. Kinking modes 1 and 3 (Cobbold & Gapais 1986) are active with little or no contribution of mode 2 (lateral migration of boundary).

(2) *Grain boundary migration* occurs when [*b*] is oriented in the stretching field. The deformation cannot be accommodated by kinking on a granular scale. A kink, in the broad sense of the Cobbold & Gapais (1986) model, does not apply in the current situation. In this investigation, monocrystals transect the whole sample with a common [*b*] direction, no process involving intracrystalline slip is able to stretch significantly the dominant slip direction in the monocrystals, and kinematic models become irrelevant. Stress and elastic energy build up rapidly in crystals and 'badly oriented' grains with higher energy are then consumed by migration of boundaries.

Acknowledgements—The authors wish to thank the Australian Research Council for their financial sponsorship of the work described in this paper. P. R. Blumenfeld was supported by a University of Melbourne Research Fellowship. J. L. Urai and W. D. Means are thanked for their thoughtful reviews of this paper.

REFERENCES

Baronnet, A. & Olives, J. 1983. The geometry of micas around kink band boundaries. I. A crystallographic model. *Tectonophysics* **91**, 359–373.

Blumenfeld, P., Mainprice, D. & Bouchez, J. L. 1986. *C*-slip in quartz from subsolidus deformed granite. *Tectonophysics* **127**, 91–115.

Bouchez, J.-L & Duval, P. 1982. The fabric of polycrystalline ice deformed in simple shear: Experiments in torsion, natural deformation and geometrical interpretation. *Textures & Microstruct.* **5**, 171–190.

Bouchez, J.-L., Lister, G. S. & Nicolas, A. 1983. Fabric asymmetry and shear sense in movement zones. *Geol. Rdsch.* **72**, 401–419.

Cobbold, P. R. & Gapais, D. 1986. Slip-system domains. I. Plane-strain kinematics of arrays of coherent bands with twinned fibre orientations. *Tectonophysics* **131**, 113–132.

Cobbold, P. R. 1977. Description and origin of banded deformation structures. I. Regional strain, local perturbations, and deformation bands. *Can. J. Earth Sci.* **14**, 1721–1731.

Cobbold, P. R., Means, W. D. & Bayly, M. B. 1984. Jumps in deformation gradients and particle velocities across propagating coherent boundaries. *Tectonophysics* **108**, 283–298.

Gapais, D. & Cobbold, P. R. 1987. Slip system domains. 2. Kinematic aspects of fabric development in polycrystalline aggregates. *Tectonophysics* **138**, 289–309.

Jessell, M. W. 1986. Grain boundary migration and fabric development in experimentally deformed octachloropropane. *J. Struct. Geol.* **8**, 527–542.

Lister, G. S., Paterson, M. S. & Hobbs, B. E. 1978. The simulation of fabric development in plastic deformation and its application to quartzite: The model. *Tectonophysics* **45**, 107–158.

Matvienko, V. N., Pertsov, N. V. & Schukin, E. D. 1979. Plasticizing of naphthalene single crystals by surface active organic media. *Mol. Cryst. Liq. Cryst.* **51**, 1–8.

McLaren, A. C. & Etheridge, M. A. 1980. A transmission electron microscope study of naturally deformed orthopyroxene. II: Mechanisms of kinking. *Bull. Mineral.* **103**, 558–563.

Means, W. D. 1981. The concept of a steady state foliation. *Tectonophysics* **78**, 179–199.

Means, W. D. 1989. Synkinematic microscopy of transparent polycrystals. *J. Struct. Geol.* **11**, 163–174.

Means, W. D., Hobbs, B. E., Lister, G. S. & Williams, P. F. 1980. Vorticity and non-coaxiality in progressive deformations. *J. Struct. Geol.* **2**, 371–378.

Means, W. D. & Jessell, M. W. 1986. Accommodation migration of grain boundaries. *Tectonophysics* **127**, 67–86.

Poirier, J.-P. 1980. Shear localization and shear instability in materials in the ductile field. *J. Struct. Geol.* **2**, 135–142.

Poirier, J.-P. 1985. *Creep of Crystals*. Cambridge University Press, Cambridge, U.K.

Ramsay, J. G. 1967. *Folding and Fracturing of Rocks*. McGraw-Hill, New York.

Ramsay, J. G. & Huber, M. I. 1987. *The Techniques of Modern*

Structural Geology, Volume 2: *Folds and Fractures*. Academic Press, London. 700 pp.
Robinson, P. M. & Scott, H. G. 1967. The effect of impurities on the deformation behaviour of naphthalene. *Acta metall.* **15**, 1230–1231.
Robinson, P. M. & Scott, H. G. 1970. Basal and non-basal slip in anthracene single crystals. *Mol. Cryst. Liq. Cryst.* **11**, 13–23.
Smith, R. B. 1975. Unified theory of the onset of folding, boudinage and mullion structure. *Bull. geol. Soc. Am.* **86**, 1601–1609.
Starkey, J. 1968. The geometry of kind bands in crystals. A simple model. *Contr. Miner. Petrol.* **19**, 133–141.
Sundararajan, K. S. 1936. Optical studies on organic crystals—Part I. *Z. Kristallogr.* **A93**, 238–248.
Taylor, G. I. 1938. Plastic strain in metals. *J. Inst. Metall.* **62**, 307–324.
Urai, J. L. 1987. Development of microstructure during deformation of carnallite and bischofite in transmitted light. *Tectonophysics* **135**, 251–263.
Urai, J. L., Means, W. D. and Lister, G. S. 1986. Dynamic recrystallization of minerals. In: *Mineral and Rock Deformation: Laboratory Studies* (edited by Hobbs, B. E. & Heard, H. C.). *Am. Geophys. Un. Geophys. Monogr.* **36**, 161–199.
Weiss, L. E. 1980. Nucleation and growth of kink bands. *Tectonophysics* **65**, 1–38.
Williams, J. O. & Thomas, J. M. 1967. Lattice imperfections in organic solids. I. Anthracene. *Trans. Faraday Soc.* **63**, 1720.
Wilson, C. J. L. 1986. Deformation induced recrystallization of ice: The application of in situ experiments. In: *Mineral and Rock Deformation: Laboratory Studies* (edited by Hobbs, B. E. & Heard, H. C.). *Am. Geophys. Un. Geophys. Monogr.* **36**, 213–232.
Wyckoff, R. W. G. 1971. *Crystal Structures* (2nd edn). Wiley, New York.